

Cite this: *Phys. Chem. Chem. Phys.*, 2012, **14**, 16111–16114

www.rsc.org/pccp

PAPER

Fabrication of n-type ZnO nanowire/graphene/p-type silicon hybrid structures and electrical properties of heterojunctions

Zhiwen Liang,^{†a} Xiang Cai,^{†b} Shaozao Tan,^b Peihua Yang,^a Long Zhang,^a Xiang Yu,^c Keqiu Chen,^a Hanming Zhu,^a Pengyi Liu^{*a} and Wenjie Mai^{*ad}

Received 30th September 2012, Accepted 15th October 2012

DOI: 10.1039/c2cp43453a

Compared to the p–n junction type device (Device A) with an n-type ZnO nanowire (n-ZnO)/p-type silicon (p-Si) hybrid structure, the newly designed device (Device B) with an n-ZnO/reduced graphene oxide sheet (rGO)/p-Si hybrid structure displays interesting electrical characteristics such as lower turn-on voltage and better current symmetry. The addition of rGO between n-ZnO and the p-Si substrate enables tuning of the p–n junctions into back-to-back Schottky junctions and lowering of the turn-on voltages, implying great potential applications in electronic and optoelectronic devices. The electrical characteristics and operating mechanism of these two devices are fully discussed.

Introduction

As one of the excellent semiconductor nanomaterials, ZnO nanostructures including nanowires,¹ nanobelts,² nanotubes,³ nanorings,⁴ and nanohelices⁵ have been extensively studied and remarkable breakthroughs have been achieved in the past decade. In 2004, a novel nanomaterial, graphene, was discovered as a single 2-dimensional carbon sheet with the same structure as the individual layers in graphite.^{6–8} So far, ZnO and graphene have individually exhibited enormous potential for applications in electronic and optoelectronic devices.^{9–12}

Although ZnO and graphene have attracted much scientific attention due to their novel and promising characteristics at the nanometer scale, studies into the properties of their hybrid structures has just started. Recently, research efforts focusing on hybrids of ZnO nanostructures and graphene as well as their potential device applications have been reported. ZnO nanorod–graphene hybrid architectures exhibiting a high current flow and distinct light emission could serve as multifunctional conductors.¹³ The transparent and flexible ZnO nanowire/graphene hybrids on a polydimethylsiloxane (PDMS) substrate show excellent field emission properties with low turn-on voltage at all convex, flat, and concave deformation situations.¹⁴

In addition, ZnO nanorods on reduced graphene oxide (rGO) electrodes have been further applied in hybrid solar cells, whose conversion efficiency is higher than that reported for previous solar cells using graphene films as electrodes.¹⁵ This progress clearly suggests that the ZnO nanostructure/graphene hybrids combining the advantages of both materials can display better performance in many device applications.

In this study, ZnO nanowires are grown directly on the cleaned p-type silicon (p-Si) substrate and these form the p–n electrical junctions with an n-type ZnO nanowire (n-ZnO)/p-Si hybrid structure (Device A). In contrast, ZnO nanowires are also grown on the rGO sheet/p-Si substrate using a similar procedure. The rGO, which is prepared by chemical exfoliation from natural graphite in oxidative aqueous dispersion and subsequent hydrazine reduction, is transferred onto the surface of the p-Si substrate. ZnO nanowires are grown on both p-Si and rGO/p-Si substrates in a heated zinc nitrate and hexamethylenetetramine mixture solution. The novel n-ZnO/rGO/p-Si hybrid (Device B) is fabricated and the heterojunction displays distinct electrical property different from the p–n junction property of the n-ZnO/p-Si hybrid structure. The addition of an rGO sheet between the n-ZnO and p-Si enables lowering of the turn-on voltages and tuning of p–n junctions into back-to-back Schottky junctions. A characteristic of these rectifying junctions is that they allow an electric current to pass in one direction while blocking or modifying the current in the opposite direction, which can be used to regulate voltage, to tune radio, and to generate radio frequency oscillations. The schematics of band structures of both devices are illustrated to explain the underlying mechanism. These two kinds of heterojunctions should find many potential applications in electronic and optoelectronic devices.

^a Department of Physics and Siyuan Laboratory, Jinan University, Guangzhou, Guangdong 510632, China.

E-mail: wenjiemai@gmail.com, tply@jnu.edu.cn

^b Department of Chemistry, Jinan University, Guangzhou, Guangdong 510632, China

^c Analytical and Testing Center, Jinan University, Guangzhou, Guangdong 510632, China

^d Key Laboratory of Optoelectronic Information and Sensing Technologies, Jinan University, Guangzhou, Guangdong 510632, China

† Z. W. Liang and X. Cai contributed equally to this work.

Experimental

Preparation of graphene oxide (GO) and rGO

GO was prepared by a modified Hammer's method as reported.¹⁶ Subsequently, the GO was ultrasonicated in water for 3 h to obtain GO sheets, followed by centrifugation for 30 min at 3000 rpm to remove any potential unexfoliated oxidized graphite. After adjusting pH to 11 by 5% ammonium hydroxide, hydrazine hydrate was then added to the GO dispersion solution (0.1 mg mL^{-1}). The resulting mixture was heated at $95\text{--}100 \text{ }^\circ\text{C}$ for 2 h under a water-cooled condenser and then cooled to room temperature. The resulting solution was then filtered through a polycarbonate membrane ($0.22 \text{ } \mu\text{m}$ pore size) and was repeatedly washed by ultrapure water. The collected rGO was redistributed in ultrapure water (ratio of 1.25 mg rGO to 1 mL water) by ultrasonication in a water bath for 15 min.

Preparation of ZnO nanowires and devices

In our experiment, a highly boron-doped p-Si (100) substrate with an electrical resistivity of $0.008 \text{ } \Omega\text{-cm}$ was used as the growth substrate. For Device B, the rGO suspension was gently released on the p-Si by a dropper in a clean room and allowed to dry in a fume hood for evaporation of the solvent. The processes were repeated until the average thickness of the as-prepared rGO sheet was about 200 nm , confirmed by a surface profiler. Subsequently, a 100 nm thick ZnO film was deposited onto the rGO sheet by a magnetron sputtering method. The nutrient solution for ZnO nanowire growth in our experiment was composed of zinc nitrate and hexamethylenetetramine at $1 : 1$ ratio with both concentrations at the same 25 mmol L^{-1} . The rGO/p-Si substrate was carefully placed on the surface of the nutrient solution with the seed layer facing downward. The nutrient solution was maintained at $90 \text{ }^\circ\text{C}$ for 28 h. The final sample was taken out and cleaned by deionized water (DI water) thoroughly and dried naturally. Scanning electron microscope (SEM) images indicated that the ZnO nanowires covered the entire surface of the substrate. The indium tin oxide (ITO) glass serving as a top electrode was firmly pressed on top of the ZnO nanowire arrays, completing the fabrication of Device B. Concerning the fabrication of Device A, the step of deposition of the rGO sheet was absent and other steps were performed exactly in the same way. Schematics of Devices A and B are illustrated in Fig. 1a and b, respectively.

Characterization

The morphology of ZnO nanowires was characterized by a field-emission scanning electron microscope (FESEM, HITACHI S-4800). The morphology of graphene was characterized by an atomic force microscope (AFM, Benyuan CSPM5500). The thickness of the graphene sheet was checked and confirmed by a surface profiler (KLA-Tencor XP-2). The crystal structures of ZnO nanowires and graphene were determined by an X-ray diffractometer (XRD) using $\text{Cu K}\alpha$ radiation (Rigaku D/max 2500v/pc). The electrical measurements were carried out using a Keithley 2635 system controlled by a computer.

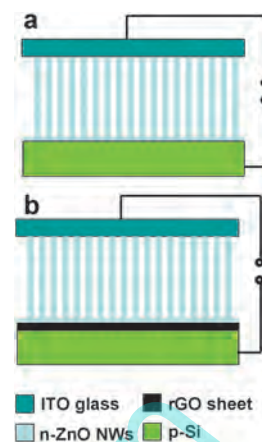


Fig. 1 (a) and (b) Schematics of the fabricated n-ZnO/p-Si hybrid structure (Device A) and n-ZnO/rGO/p-Si hybrid structure (Device B), respectively.

Results and discussion

Fig. 2a shows the SEM image of ZnO nanowires, whose growth orientations are random. The typical length of the ZnO nanowires is $4\text{--}5 \text{ } \mu\text{m}$, the diameter is $80\text{--}100 \text{ nm}$, and the density is $\sim 45 \text{ } \mu\text{m}^{-2}$. Fig. 2b displays the XRD patterns of graphite, rGO, and ZnO nanowires grown on the rGO (ZnO + rGO). While the sharp and intensive peak at $2\theta = 26.4^\circ$ for graphite indicates a highly organized crystal structure with the (002) interlayer spacing of 0.337 nm , the low and broad peak at $2\theta = 24.8^\circ$ for rGO represents the (002) interlayer spacing of 0.359 nm . The slight expansion of interlayer spacing is regarded to result from the residual functional groups that may exist between the rGO layers. The low XRD signal-to-noise ratio of peak (002) for rGO is because the exfoliated graphene was stacked weakly during the fabrication. Since the thickness of the rGO sheet where ZnO nanowires grow is only 200 nm , the (002) peak from rGO is too weak to be observed in this ZnO + rGO sample. However, the peaks of (002) and (101) from ZnO nanowires are strong and sharp, demonstrating the excellent crystallinity of ZnO nanostructures and bestowing their candidacy for electronic applications. Our previous research results demonstrated that the ZnO nanowires obtained by this solution reaction method are grown along c direction, so the appearance of the ZnO (101) peak suggests the random orientation of ZnO nanowires.¹⁷

The AFM image and cross-section profile analysis of the as-prepared rGO on a flat mica substrate are shown in Fig. 3a and b. The thickness of the as-prepared rGO is about 0.7 nm ,

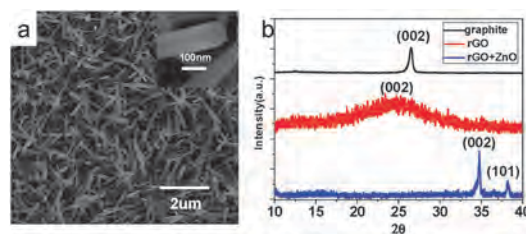


Fig. 2 (a) SEM image of ZnO nanowires grown on an rGO sheet by a wet chemical method (15° view). The inset is the enlarged SEM image. (b) XRD patterns of graphite, rGO, and ZnO nanowires (grown on rGO).

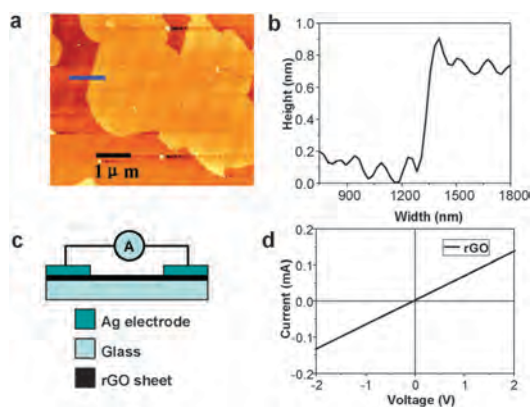


Fig. 3 (a) The tapping-mode AFM image of the as-prepared rGO on a clean mica surface. (b) The cross-sectional profile of rGO sample indicated by a blue line in (a). (c) Schematic of the electrical characterization system of the 200 nm thick rGO sheet. (d) Electrical I - V curve of the rGO sheet suggesting its metallic property.

suggesting that our rGO has 1–2 layers of carbon atoms. Although the area of a single layer of rGO varies from a few micrometer squares to thousands of micrometer squares, rGO is unable to cover the entire $1 \times 1 \text{ cm}^2$ substrate with only a single layer. Therefore, a large amount of rGO was repeatedly deposited on the p-Si substrate, forming a 200 nm thick rGO sheet, to ensure the entire coverage by rGO and no current leakage between ZnO nanowires and the p-Si substrate in Device B.

The electrical properties of the as-prepared nanomaterials and devices were characterized by an I - V measurement system (Keithley 2601) at room temperature. Fig. 3c illustrates the experimental setup for electrical measurement and Fig. 3d displays the I - V curve obtained from a 200 nm thick rGO sheet separated by two Ag electrodes with a 2 mm gap, which were deposited on the rGO sheet by silver paste. The nearly linear current response to the applied voltage suggests that the rGO sheet with good conductivity is metallic. The excellent conductivity of the as-prepared rGO can play an important role in the electronic devices. Fig. 4a and b show the electrical properties of Device A with an n-ZnO/p-Si structure and Device B with an n-ZnO/rGO/p-Si structure, respectively. The positive voltage in Fig. 4 means that p-Si was positively biased. Two distinct differences are observed in their I - V curves. Firstly, Device A displays rectifying behavior of typical p–n junctions, which was previously observed in other work.¹⁸ Instead of significantly blocking the reverse currents as in p–n junctions in Device A, the reverse energy barrier of Device B seems to be highly reduced, inducing a significantly larger reverse current. Secondly, the turn-on voltages

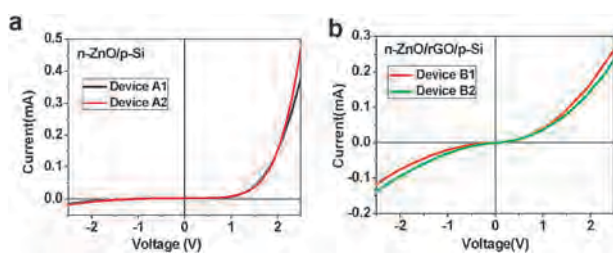


Fig. 4 (a) Rectifying I - V characteristics for the n-ZnO/p-Si hybrid structure (Device A). (b) Rectifying I - V characteristics for a novel n-ZnO/rGO/p-Si hybrid structure (Device B).

Table 1 The forward and reverse turn-on voltages of Device A and Device B at 0.1 mA

Device no.	Forward turn-on voltage (V)	Reverse turn-on voltage (V)
A1	1.82	—
A2	1.84	—
B1	1.56	2.33
B2	1.68	2.06

(current at 0.1 mA) of the two kinds of devices are different and listed in Table 1. The turn on voltages of Device B when forwardly biased are ~ 1.6 V, systematically lower than those of Device A at ~ 1.8 V, implying the presence of a slight barrier introduced by the rGO sheet. The discovery of the new electrical characteristics of Device B enriches the functionality of semiconductor-based devices, and may have great implications for future graphene-based applications.

In order to understand the underlying physics of these two kinds of devices, the possible underlying mechanism is discussed in detail below. The original band diagrams of individual p-Si, rGO, and ZnO are plotted in Fig. 5a. For Device A, when the n-ZnO nanowires are grown on the p-Si substrate forming a p–n diode, the energy band diagram under equilibrium conditions is illustrated in Fig. 5b, where the Fermi level is a constant independent of position, leading to a “build-in” voltage V_{bi} across the junction. When a positive bias V_{app} is applied on the p-Si, the forward bias band diagram is plotted by moving the n-ZnO side upward by qV_{app} while holding the p-Si side fixed, as shown in Fig. 6a. It is readily established that

$$E_{Fp} - E_{Fn} = -eV_{app}$$

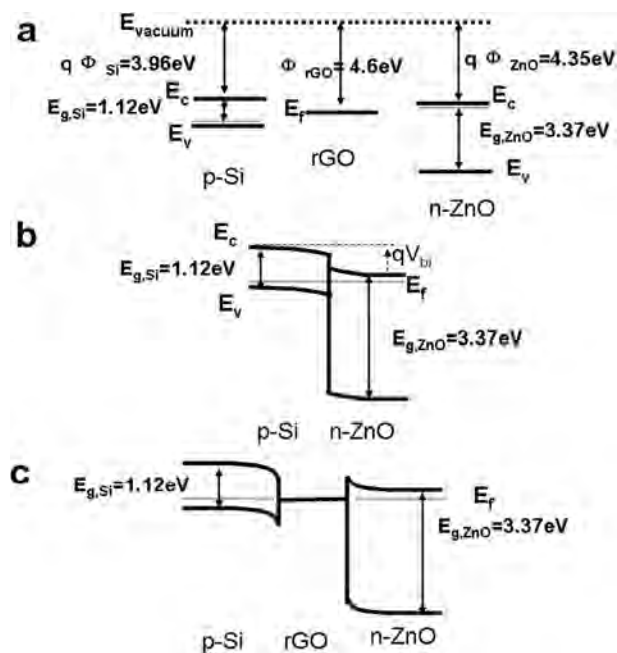


Fig. 5 (a) Individual band diagrams of the p-Si substrate, rGO sheet, and n-ZnO nanowires. (b) The energy diagram of an n-ZnO/p-Si heterojunction (Device A) under equilibrium conditions. (c) The energy diagram of an n-ZnO/rGO/p-Si hybrid heterostructure (Device B) under equilibrium conditions.

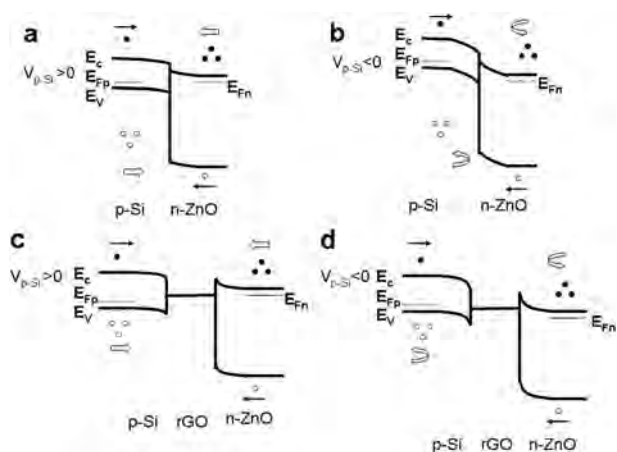


Fig. 6 (a) and (b) Band diagrams of an n-ZnO/p-Si heterojunction (Device A) under positive and negative biased conditions, respectively. (c) and (d) Band diagrams of an n-ZnO/rGO/p-Si hybrid heterostructure (Device B) under positive and negative biased conditions, respectively.

where E_{Fp} and E_{Fn} are majority-carrier quasi-Fermi levels of p-Si and n-ZnO, respectively.

The larger the V_{app} applied, the lower the energy barrier and the thinner the depletion width between the diodes. In contrast, a negative bias will induce a higher energy barrier and a thicker depletion width as shown in Fig. 6b. Therefore, Device A permits a net flow of electrons from n-ZnO to the p-Si substrate and the increasing V_{app} leads to a rapidly rising forward bias current. On the other hand, even the minority-carrier electrons in p-Si are all pulled through the junction by the reverse bias, the associated reverse-bias current should be relatively small. The above statements well explain the features in Fig. 4a. For Device B, the existence of the rGO layer between n-ZnO and the p-Si substrate modifies the junction and its corresponding electrical properties. The energy band diagram of Device B under equilibrium conditions is illustrated in Fig. 5c, where two Schottky junctions are formed back-to-back in series. Schottky junctions fall into the category of metal–semiconductor junctions, but the rectifying Schottky behavior appears only if $\Phi_M > \Phi_S$ for n-type semiconductors and $\Phi_M < \Phi_S$ for p-type semiconductors, where Φ_M and Φ_S are the workfunctions of metals and semiconductors, respectively. Here in Device B, the rGO can be regarded as a metal with good conductivity,¹⁹ constructing Schottky diodes individually with p-Si and n-ZnO because of their different workfunctions.²⁰ Comparing with p–n junctions in Device A, the lower forward turn-on voltages can be found in Schottky diodes in Device B due to the smaller built-in potential, the larger reverse currents and the much lower reverse turn-on voltages, as shown in the band diagram under an applied voltage in Fig. 6c and d. The forward and reverse turn-on voltages are listed in Table 1, which suggest the large differences between the two kinds of devices. As an inherent property, the low reverse turn-on voltage and large reverse current of Schottky diodes are reflected in the negative biased I – V curves of Device B in Fig. 4b. The surface absorption and contamination on n-ZnO/rGO/p-Si Schottky diodes also contribute to the above mentioned phenomenon, thus the I – V curves of Device B do not have a significant blocking effect. From the experiment and discussion above, it can be seen that the existence of rGO has changed the

nature of the heterojunctions and tuned the device transport properties from p–n behavior to Schottky behavior.

Conclusions

We have successfully fabricated and electrically characterized a novel hybrid structure of n-ZnO/rGO/p-Si. Compared to the p–n hybrid structure of n-ZnO/p-Si, our new one indicates that the rGO between n-ZnO and the p-Si substrate could tune the contact electrical property from p–n junctions to back-to-back Schottky junctions and enrich the variations and functionalities of the devices, therefore rGO may find great potential applications in fabricating electronic and optoelectronic devices.

Acknowledgements

This work is financially supported by the National Natural Science Foundation of China (Grant No. 51102115), the Specialized Research Fund for the Doctoral Program of Higher Education of China (Grant No. 20104401120005), the Key Project of Chinese Ministry of Education (Grant No. 211208), and Fundamental Research Funds for the Central Universities (Grant No. 21612109).

Notes and references

- 1 L. Vayssieres, *Adv. Mater.*, 2003, **15**, 464–466.
- 2 S. H. Yang, X. G. Wen, Y. P. Fang, Q. Pang, C. L. Yang, J. N. Wang, W. K. Ge and K. S. Wong, *J. Phys. Chem. B*, 2005, **109**, 15303–15308.
- 3 M. Y. Han, H. D. Yu, Z. P. Zhang, X. T. Hao and F. R. Zhu, *J. Am. Chem. Soc.*, 2005, **127**, 2378–2379.
- 4 Z. L. Wang, X. Y. Kong, Y. Ding and R. Yang, *Science*, 2004, **303**, 1348–1351.
- 5 Z. L. Wang, R. S. Yang and Y. Ding, *Nano Lett.*, 2004, **4**, 1309–1312.
- 6 A. Hashimoto, K. Suenaga, A. Gloter, K. Urita and S. Iijima, *Nature*, 2004, **430**, 870–873.
- 7 K. S. Novoselov, A. K. Geim, S. V. Morozov, D. Jiang, Y. Zhang, S. V. Dubonos, I. V. Grigorieva and A. A. Firsov, *Science*, 2004, **306**, 666–669.
- 8 K. S. Novoselov, A. K. Geim, S. V. Morozov, D. Jiang, M. I. Katsnelson, I. V. Grigorieva, S. V. Dubonos and A. A. Firsov, *Nature*, 2005, **438**, 197–200.
- 9 K. Chung, C. H. Lee and G. C. Yi, *Science*, 2010, **330**, 655–657.
- 10 F. Bonaccorso, Z. Sun, T. Hasan and A. C. Ferrari, *Nat. Photon.*, 2010, **4**, 611–622.
- 11 L. J. Zhi, X. Wang and K. Mullen, *Nano Lett.*, 2008, **8**, 323–327.
- 12 D. Choi, M. Y. Choi, W. M. Choi, H. J. Shin, H. K. Park, J. S. Seo, J. Park, S. M. Yoon, S. J. Chae, Y. H. Lee, S. W. Kim, J. Y. Choi, S. Y. Lee and J. M. Kim, *Adv. Mater.*, 2010, **22**, 2187–2192.
- 13 W. I. Park, J. M. Lee, Y. B. Pyun, J. Yi and J. W. Choung, *J. Phys. Chem. C*, 2009, **113**, 19134–19138.
- 14 S. O. Kim, J. O. Hwang, D. H. Lee, J. Y. Kim, T. H. Han, B. H. Kim, M. Park and K. No, *J. Mater. Chem.*, 2011, **21**, 3432–3437.
- 15 H. Zhang, Z. Y. Yin, S. X. Wu, X. Z. Zhou, X. Huang, Q. C. Zhang and F. Boey, *Small*, 2010, **6**, 307–312.
- 16 R. E. Offeman, Jr. and W. Hummers, *J. Am. Chem. Soc.*, 1958, **80**, 1339.
- 17 S. Xu, Y. Wei, M. Kirkham, J. Liu, W. Mai, D. Davidovic, R. L. Snyder and Z. L. Wang, *J. Am. Chem. Soc.*, 2008, **130**, 14958–14959.
- 18 Y. B. Hahn, N. K. Reddy, Q. Ahsanulhaq and J. H. Kim, *Appl. Phys. Lett.*, 2008, **92**, 043127.
- 19 Y. W. Zhu, S. Murali, W. W. Cai, X. S. Li, J. W. Suk, J. R. Potts and R. S. Ruoff, *Adv. Mater.*, 2010, **22**, 3906–3924.
- 20 X. W. Sun, S. T. Tan, J. L. Zhao, S. Iwan, Z. H. Cen, T. P. Chen, J. D. Ye, G. Q. Lo, D. L. Kwong and K. L. Teo, *Appl. Phys. Lett.*, 2008, **93**, 013506.